Theory of Magnetoelectric Effects in Multiferroic Core-Shell Nanofibers of Hexagonal Ferrites and Ferroelectrics

V. M. Petrov,[1,2] Jitao Zhang,[1,3] Hongwei Qu,[4] Peng Zhou,[1,5] Tianjin Zhang,[5] and G. Srinivasan[1a)]

[1] *Physics Department, Oakland University, Rochester, MI 48309, USA*

[2] *Institute of Electronic and Information Systems, Novgorod State University, Veliky Novgorod 173003, Russia*

[3] *College of Electrical and Information Engineering, Zhengzhou University of Light Industry, Zhengzhou 450002, People's Republic of China*

[4] *Electrical and Computer Engineering, Oakland University, Rochester, MI 48309, USA*

[5]*Department of Materials Science and Engineering, Hubei University, Wuhan 430062, China*

ABSTRACT

A models is developed for magneto-electric (ME) interactions in coaxial nano-fibers of hexagonal ferrites and ferroelectrics. Multiferroic nanocomposites with hexagonal ferrites are of interest for achieving strong ME coupling under zero external magnetic bias due to their high uniaxial or planar anisotropy field. In this work we considered the ME coupling in core-shell fibers of lead zirconate titanate (PZT) and ferrimagnetic W- and Y-type hexagonal ferrites with high magnetostriction and piezomagnetic coupling. Modeling of the direct- ME effects, i.e., sample response to an applied magnetic field, is done in terms of the ME voltage coefficients (MEVC) at low frequencies and at electromechanical resonance (EMR). The converse-ME effect, response of the fibers to an applied DC electric field, is considered at ferromagnetic

resonance (FMR). Expressions have been obtained for MEVC at low-frequency and EMR and for the converse ME coefficient at FMR. The theory predicts strongest direct-ME coupling in fibers of Ni_2Y-PZT and the weakest coupling in Zn_2Y-PZT. The MEVC at EMR is one to two orders of magnitude higher than at low-frequency and the peak MEVC remains the same for fibers of ferrite core-PZT shell as for PZT core-ferrite shell. The converse ME effect is expected to be the strongest for fibers of Co_2W-PZT and weakest in Ni_2Y-PZT. The model has been extended to include an assembled array of core-shell fibers and weakening of the ME coupling is predicted in such arrays due to magnetic and electric dipole-dipole interactions. The theory presented here is of importance for self-biased sensors of low frequency and RF magnetic fields.

a) Corresponding author email: srinivas@oakland.edu

1. Introduction

Single-phase and composite multiferroics are of interest for studies on the coupling between magnetic and electric subsystems and for sensors and dual magnetic and electric field controlled device technologies [1-13]. In such materials the magnetoelectric (ME) interactions lead to an induced polarization in an applied magnetic field or an induced magnetization/anisotropy field in an electric field. A majority of single-phase ME materials exhibit either a weak ME coupling at room temperature or strong coupling at very low temperatures [1-3]. Composites of magnetostrictive and piezoelectric phases, however, show strong ME interactions that arises due mechanical deformation in an applied magnetic or electric field [4-8]. Several layered composites with lead zirconate titanate (PZT), lead magnesium niobate-lead titanate (PMN-PT), lanthanum gallium tantalate (LGT) or quartz for the ferroelectric/piezoelectric phase and 3d-transition metals or alloys or ferrites for the magnetostrictive phase were found to show strong ME coupling at room temperature [8-10].

In multiferroic nanocomposites such as nanobilayers and core-shell fibers one expects strengthening of strain mediated ME interactions due to a large surface area-to-volume ratio that is orders of magnitude higher than for thick film layered composites. Nanostructures studied so far include bilayers, core-shell particles, nanopillars, and core-shell fibers. Synthesis of core-shell particles of ferrites and ferroelectrics by techniques including hydrothermal annealing process were reported [14,15]. In another study particles of barium titanate (BTO) and cobalt ferrite were functionalized by attaching complementary chemical coupling groups and a core-shell particulate composite was formed by covalent bonds between the two particles [16]. We recently reported on chemical self-assembly and DNA-assisted assembly of core-shell particles of nickel ferrite (NFO) and BTO [17,18]. Coaxial NFO-PZT or BTO nanowires were synthesized by techniques including electrospinning [21-23]. The fibers were assembled into *2D* and *3D* films with magnetic and/or electric fields [23]. Strong ME interactions in core-shell

particles and coaxial wires were evident from measurements of low-frequency ME effect, magnetic field induced-induced polarization, and magneto-dielectric effects at 1-40 GHz [23-25].

Ferromagnetic-ferroelectric nanocomposites such as bilayers and multilayers were studied in recent years. Systems studied include nanobilayers on a substrate or ferromagnetic (ferroelectric) films deposited directly on ferroic substrates. Synthesis of nanopillars of ferrites in BTO, PZT, or $BiFeO_3$ matrix were reported by several techniques including pulsed laser deposition [19,20]. Although pulsed laser deposition (PLD) was used extensively for bilayer synthesis, techniques such as RF sputtering, spin coating and atomic layer deposition were also used. The ferroic heterostructures on substrates in general are expected to have weak ME coupling due to substrate clamping and the loss of field induced mechanical strain at the interface. Composites of nanopillars on a host matrix attracted attention in this regard since substrate clamping could potentially be eliminated in such structures [19,20]. A giant converse ME effect was reported for nickel zinc ferrite-BTO [19] and $BiFeO_3$-cobalt ferrite-PMN-PT nanopillars systems [20].

This work is on the theory of ME effects in core-shell multiferroic nanofibers. Theory of ME interactions in nanocomposites is of importance for selection of appropriate ferroic phases and for optimizing the nanostructures to achieve the expected strong ME coupling. We modeled ME coupling at low frequencies and at electromechanical resonance (EMR) in spinel ferrite-ferroelectric nanobilayers, nanopillars and core-shell fibers [26,27]. The low-frequency coupling in BTO-NFO core-shell fibers, for example, is predicted to be almost an order of magnitude higher than for thin film composites if the fiber length is large compared to its radius [26]. An enhancement in the strength of ME coupling by an order of magnitude or more at EMR compared to low frequency coupling is expected for BTO-NFO coaxial fibers [27]. We also extended the model to include ME coupling at magnetoacoustic resonance, i.e., at the overlap

of EMR and ferromagnetic resonance (FMR) and theory predicts an order of magnitude higher ME voltage at MAR compared to EMR. We were able to confirm the predicted strong ME coupling in core-shell spinel ferrite-piezoelectric nanowires [23].

Here we discuss results of our modeling of ME coupling in coaxial nanofibers of hexagonal ferrites and piezoelectric PZT. Ferrimagnetic hexagonal ferrites, in general, consist of spinel (S) blocks and hexagonally packed R or T blocks containing divalent Ba or Sr. Antiferromagnetic alignment of Fe^{3+} gives rise to a net magnetization and the ferrites show very high uniaxial anisotropy field, 10-20 kOe, along the hexagonal c-axis or easy plane anisotropy perpendicular to c-axis [28]. There are several types of hexaferrites, named M-, U-, W-, X-, Y, and Z-types depending on the nature of the crystal structure [29]. Since composites of PZT and M-type Ba- and Sr- ferrites have weak ME interactions due to low magnetostriction and piezomagnetic coefficient, they are not considered in this work [7]. Hexaferrites of interest for this report are W-type and Y-type ferrites with high magnetostriction λ and piezomagnetic coefficient $q = d\lambda/dH$, key ingredients for strong ME interactions. Most of the ferromagnetic materials have $q \sim 0$ for external bias magnetic field $H = 0$. Ferromagnetic-piezoelectric composites, therefore, generally show strong ME coupling only under an external bias field [3-9]. W- and Y-type hexaferrites, however, have a large remnant magnetization that acts as self-biasing field [28, 29] and their use in a composite with PZT will result in a strong ME response under zero-bias. The response of a core-shell composite to an applied magnetic field, i.e., the direct ME effect, has been modeled in this work in terms of the ME voltage coefficients α_E at low frequencies and at frequencies corresponding to electromechanical resonance. The ME voltage coefficients have been estimated for magnetic field orientations along the fiber axis to minimum demagnetizing fields and maximum α_E. Among the system considered the highest ME coefficient of 170 V/(cm Oe) is predicted for PZT core-Ni_2Y shell and Ni_2Y core-PZT shell

nanofibers at EMR. The sample response to an applied electric field *E*, the converse ME effect, is considered at the ferromagnetic resonance (FMR) for the ferrite and the strength of ME coupling is determined by *E*-induced shift in FMR resonance field. The strongest converse ME effect is expected for fibers of Co_2W-PZT. We also considered the ME coupling in an assembly of hexaferrite core-piezoelectric shell nanofibers. The low-frequency ME voltage coefficient is predicted to increase with increasing PZT shell thickness that is accounted for by an increase in ferrite core separation with increasing shell thickness and to a decrease in the magnetic dipole-dipole interactions.

2. ME Coupling in Hexaferrite-PZT Core-Shell Fibers

The hexagonal ferrites considered in this study and their key magnetic and material parameters and parameters assumed for PZT are listed in Table 1. W-type ferrites of the composition $Ba\,Me_2\,Fe_{16}\,O_{27}$ with divalent Me = Zn or Co, namely, Zn_2W and Co_2W, and Y-type ferrites, $Ba_2\,Me_2\,Fe_{12}\,O_{22}$ (Me = Zn, Ni) (Zn_2Y and Ni_2Y) have high magnetostriction λ and piezomagnetic coefficient $q = d\lambda/dH$. Single crystals of the W-type ferrites, Zn_2W and Co_2W, have uniaxial anisotropy field H_A = 12.5 kOe and 21 kOe, respectively [28]. The Y-types, Zn_2Y and Ni_2Y, have in-plane anisotropy field of 9 kOe and 14 kOe, respectively [28,29]. Polycrystalline nanofibers of these systems are expected to show a significant remnant magnetization that acts as self-biasing field and facilitate strong ME coupling in the absence of an external bias [29].

Table 1. Material parameters for piezoelectric PZT and magnetostrictive hexagonal ferrites [28]

Material	ρ (g/cm^3)	s_{11} (10^{-12} m^2/N)	$4\pi M$ (kGs)	λ (10^{-6})	q_{33} (10^{-12} m/A)	d_{33} (10^{-12} m/V)	$\varepsilon_{33}/\varepsilon_0$

PZT	7.5	15.3		-	-	400	1750
Co_2W	5.31	6.5	2.3	-74	-170	-	10
Zn_2W	5.38	6.5	1.5	-15	-20	-	10
Zn_2Y	5.46	6.5	2.58	-10	-7	-	10
Ni_2Y	5.4	6.5	7.51	-19	-625	-	10

2.1 ME coupling at low-frequency and electromechanical resonance

A fiber with the piezoelectric core and magnetostrictive shell as in Fig.1 with length L much greater than its radius ${}^{m}R$ is considered. The fiber is subjected to an ac magnetic field of frequency f along the fiber axis (z-direction or direction *3*). In this case, demagnetization effects vanish. The PZT layer is assumed to be poled along the z-direction. The resulting deformation due to piezomagnetic effects in the ferrite is transferred to PZT resulting in a voltage response.

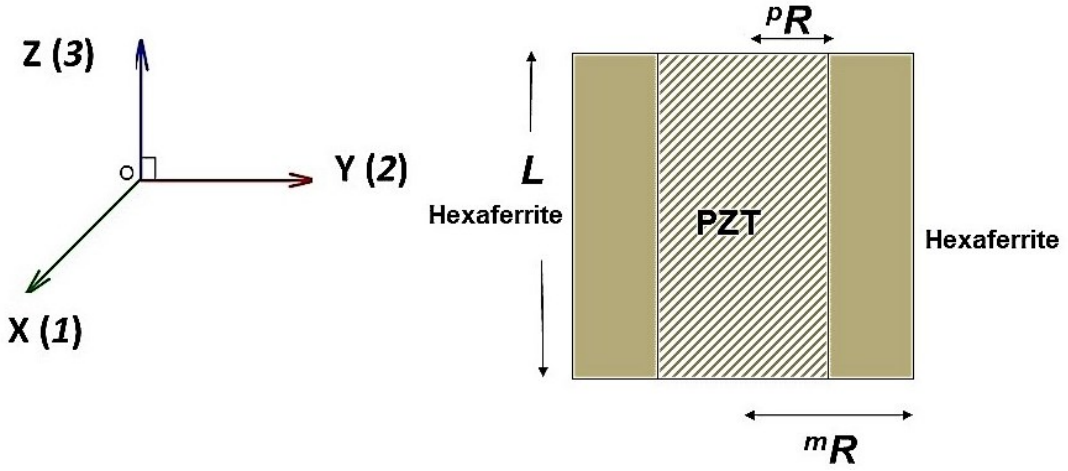

Fig. 1. Schematic diagram showing a coaxial nanofiber of length L with a core of lead zirconate titanate (PZT) of radius ${}^{p}R$ and a shell of hexagonal ferrite of outer radius ${}^{m}R$. The coordinate system [X (1), Y (2), Z (3)] used in this study is also shown.

For ME coupling at EMR we solve the equation of motion of acoustic waves in the fiber taking into account the magnetostatic and elastostatic equations, material equations, the Hooke's law,

and boundary conditions. The ME voltage coefficient which is the ratio of induced electric field to applied magnetic field is estimated. The model can be used to estimate the ME coefficients from known material parameters (piezoelectric coefficients, magnetostriction, stiffness, etc.,) [30-32].

The following *1-D* approximation of constitutive equations can be written for a nanofiber subjected to an ac magnetic field along the *z*-direction (also direction *3*) [32]:

$$
\begin{aligned}
{}^{p}S_3 &= {}^{p}s^{D}_{33}\,{}^{p}T_3 + {}^{p}g_{33}\,{}^{p}D_3\,; \\
{}^{p}E_3 &= -\,{}^{p}g_{33}\,{}^{p}T_3 + 1/{}^{p}\varepsilon_{33}\,{}^{p}D_3; \\
{}^{m}S_3 &= {}^{m}s^{B}_{33}\,{}^{m}T_3 + {}^{m}h_{33}\,{}^{m}B_3\,; \\
{}^{m}H_3 &= -\,{}^{m}h_{33}\,{}^{m}T_3 + 1/{}^{m}\mu_{33}\,{}^{m}B_3;
\end{aligned}
\qquad (1)
$$

where S_3 and T_3 are strain and stress tensor components, E_3 and D_3 are the vector components of induced electric field and electric displacement, H_3 and B_3 are the vector components of applied ac magnetic field and ac magnetic induction, respectively. The terms $h_{33} = q_{33}/\mu_{33}$ and $g_{33} = d_{33}/\varepsilon_{33}$ are piezomagnetic and piezoelectric coefficients, respectively, ε_{33} is the permittivity and μ_{33} is the permeability, s^{D}_{33} and s^{B}_{33} are the compliance coefficients at constant electric or magnetic induction. The superscripts *p* and *m* correspond to piezoelectric and piezomagnetic phases, respectively.

The equation of medium motion for the fiber has the form [27]:

$$\frac{\partial^2 u_3}{\partial z^2} = -k^2 u_3\,, \qquad (2)$$

where u_3 is displacement in direction *z*. The wavenumber *k* is defined by the expression:

$$k = \omega\sqrt{\left[{}^{p}\rho\, v + {}^{m}\rho(1-v)\right]\left[\frac{v}{{}^{p}s^{D}_{33}} + \frac{1-v}{{}^{m}s^{B}_{33}}\right]^{-1}} \qquad (3)$$

with *v* denoting the piezoelectric volume fraction and $\omega = 2\pi f$ (*f* is the frequency of ac

magnetic field). The boundary conditions have the following form for a free-standing fiber:

$^{p}T_3 v + {}^{m}T_3 (1-v) = 0$ at $z=L$;

$^{p}T_3 v + {}^{m}T_3 (1-v) = 0$ at $z=0$. (4)

Solving the medium motion for the nanofiber by taking into account Eqs. (3) – (4) and open circuit condition enables obtaining the following expression for ME voltage coefficient $\alpha_{E\,33}$.

$$\alpha_{E\,33} = \frac{2\tan(kL/2)\,{}^{p}d_{33}\,{}^{m}q_{33}r_p^2(1-r_p^2)}{kL[{}^{p}\varepsilon_{33}r_p^2+{}^{m}\varepsilon_{33}(1-r_p^2)][{}^{p}s_{33}(1-r_p^2)+{}^{m}s_{33}r_p^2]}; \quad (5)$$

where $r_p={}^{p}R/{}^{m}R$. For simplicity, electromechanical and magnetomechanical coupling coefficients are assumed to be small compared to unity.

For a fiber with the ferrite core and PZT shell, expression for ME voltage coefficient can be obtained using a similar procedure and is given by:

$$\alpha_{E,33} = \frac{2\tan(kL/2)\,{}^{p}d_{33}\,{}^{m}q_{33}r_m^2(1-r_m^2)}{kL[{}^{p}\varepsilon_{33}(1-r_m^2)+{}^{m}\varepsilon_{33}r_m^2][{}^{p}s_{33}r_m^2+{}^{m}s_{33}(1-r_m^2)]} \quad (6)$$

with $r_m={}^{m}R/{}^{p}R$. Expressions for low-frequency ME voltage coefficient under 1-*D* approximation can be obtained from Eqs. (5) and (6) and the condition that $k \to 0$ or $\omega \to 0$. We obtained the following expressions for the piezoelectric core/ferrite shell (Eq. 7) and ferrite core/piezoelectric shell (Eq. 8) fibers assuming the fiber radius to be small compared to its length:

$$\alpha_{E\,33} = \frac{{}^{p}d_{33}\,{}^{m}q_{33}r_p^2(1-r_p^2)}{[{}^{p}\varepsilon_{33}r_p^2+{}^{m}\varepsilon_{33}(1-r_p^2)][{}^{p}s_{33}(1-r_p^2)+{}^{m}s_{33}r_p^2]}, \quad (7)$$

$$\alpha_{E\,33} = \frac{{}^{p}d_{33}\,{}^{m}q_{33}r_m^2(1-r_m^2)}{[{}^{p}\varepsilon_{33}(1-r_m^2)+{}^{m}\varepsilon_{33}r_m^2][{}^{p}s_{33}r_m^2+{}^{m}s_{33}(1-r_m^2)]}. \quad (8)$$

Estimated low-frequency ME voltage coefficient (MEVC) $\alpha_{E,33}$ as a function of r_p = ratio of radius of PZT core-to-ferrite shell are shown in Fig. 2. The estimates are for fibers with PZT core and shell of W- or Y- type hexaferrites. The MEVC increases with increasing r_p and has a

maximum at r_p=0.25 that corresponds to PZT volume fraction of 0.063.

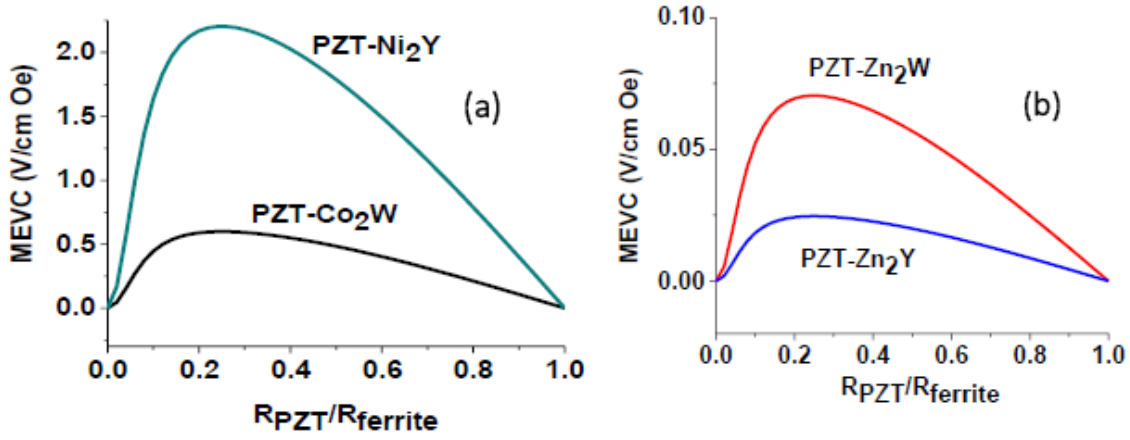

Fig. 2. Low-frequency ME voltage coefficient $\alpha_{E,33}$ as a function of r_p = ratio of core radius -to-shell radius for nanofibers of PZT core and shells of (a) Co_2W- and Ni_2Y-type hexaferrites and (b) Zn_2W and Zn_2Y.

MEVC decreases with further increase in r_p and vanishes for r_p =1. The strongest ME interactions are expected for fibers with Ni_2Y shell and the weakest for fibers with Zn_2Y. The maximum in MEVC-values in Fig.2 scales with the magnitude of the piezomagnetic coefficient q_{33} for the hexaferrites (Table 1).

Figure 3 shows similar estimates of MEVC for fibers with ferrite core and PZT shell. The dependence of MEVC on the specific choice of the ferromagnetic core is the same as for fibers with PZT core and ferrite shell. The maximum in MEVC occurs for ratio of core-to-shell radius r_m = 0.97 that corresponds PZT volume fraction of 5.91%, close to PZT volume of 6.3% for fibers with PZT core and ferrite shell. The maximum MEVC of 2.25 V/cm Oe is for fibers with Ni_2Y and minimum of 20 mV/cm Oe for fibers with Zn_2Y. Both W- and Y-hexaferrites with Zn will have a much smaller MEVC than for fibers with Ni_2Y or Co_2W.

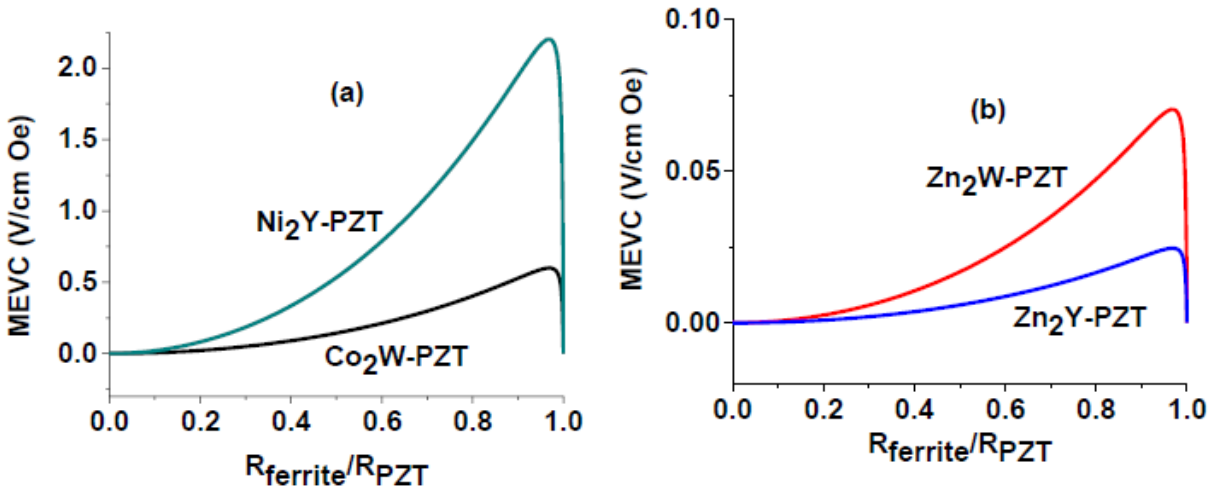

Fig. 3. Low-frequency ME voltage coefficient $\alpha_{E,33}$ as a function of r_m = ratio of ferrite core radius -to- PZT shell radius for nanofibers of ferrite core-PZT shell for a series of W- and Y-type hexaferrites.

Next we consider ME coupling at the electromechanical resonance. A significant enhancement in ME voltage coefficient is expected when the applied ac magnetic field frequency is tuned to EMR frequency [4-7]. Here we consider the longitudinal mode along the fiber length. The ME voltage coefficient was estimated using Eqs. (5) and (6). We assumed a Q-factor of 200 for the EMR mode. The ME voltage coefficient as a function of frequency is shown in Figs. 4 and 5 for fibers of length L = 1 μm and radius $R << L$. Results for nanostructures of PZT core- hexaferrite shell for a series of $r_p = R_{PZT}/R_{ferrite}$ are shown in Fig. 4. A peak in the MEVC is expected at the EMR frequency with the highest value of 170 V/cm Oe for fibers with Ni_2Y core and the smallest value of 1.8 V/cm Oe for fibers with Zn_2Y core. Fibers with r_p=0.4 is predicted to have the maximum value at 2.65 GHz and differs from r_p=0.25 for maximum MEVC at low frequencies (Fig.2) and is due to the dependence of high frequency MEVC on wavenumber k (Eq.5).

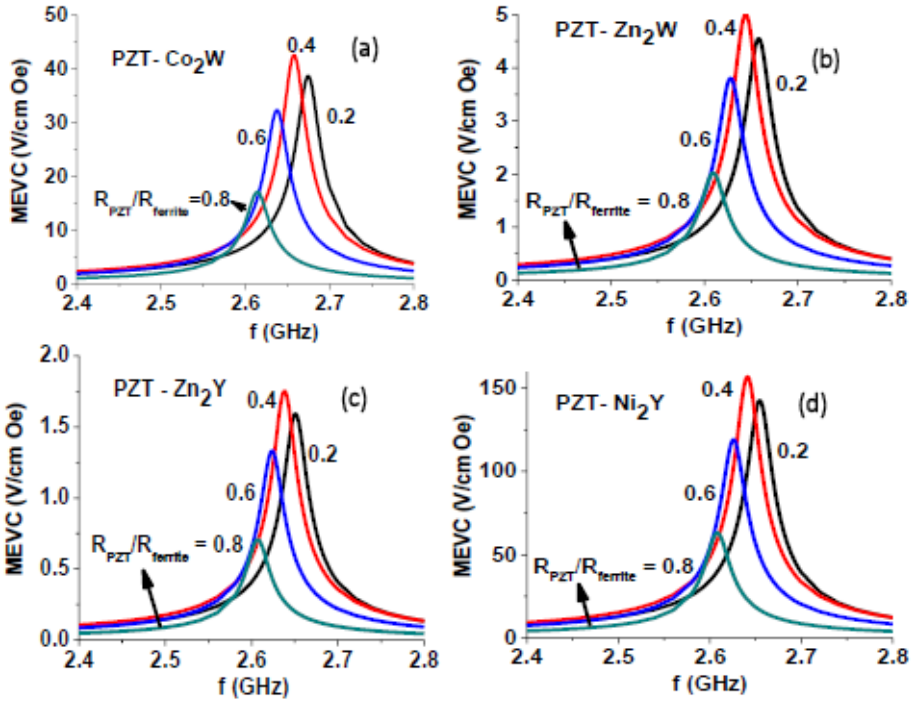

Fig.4: Frequency dependence of ME voltage coefficient for fibers of PZT core- hexaferrite of 1 μm for a series of ratio of core-to-shell radius.

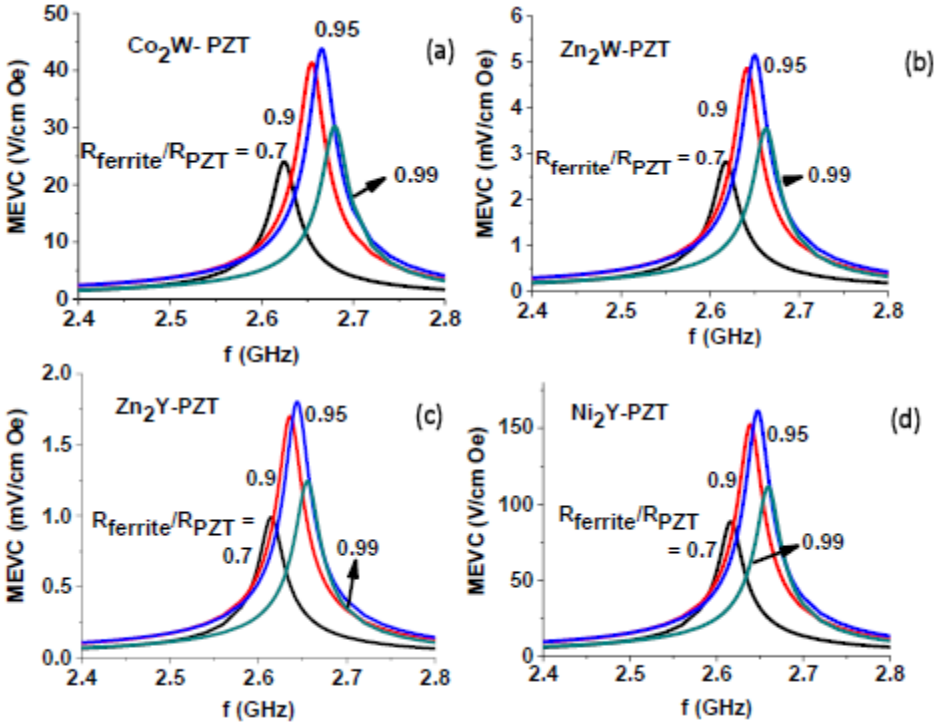

Fig.5: Frequency dependence of ME voltage coefficient for hexaferrite core-PZT shell fibers of length 1 μm. Results are shown for a series of ratio of core radius to shell radius.

Figure 5 shows similar frequency dependence of MEVC for fibers with ferrite core and PZT shell for r_m = 0.7 to 0.99. The maximum in ME voltage coefficient is estimated for r_m = 0.95 and differs from the maximum value for r_p = 0.4 for fibers with PZT core and ferrite shell. The peak MEVC at the resonance frequency of 2.65 GHz in Fig.5, however, remains the same as for fibers with PZT core. Fibers with Ni_2Y core has the highest MEVC whereas those with Zn_2Y core has the weakest ME response.

In section 3 we discuss in detail results in Figs.2-5 on direct ME effects in core-shell fibers and their significance.

2.2 Magnetoelectric Effect at Ferromagnetic Resonance

The converse ME effect in the core-shell structures is discussed next [5-9]. A core-shell fiber when subjected to an electric field E is expected to show a shift in the FMR field/frequency due to piezoelectric strain. The shift δH_E in the FMR field due to E is estimated and the ME coefficient $\alpha_H = \delta H_E/E$ is determined [9]. We consider a ferrite-piezoelectric nanofiber as in Fig.1 with a self-bias or an applied bias field $\boldsymbol{H_0}$ along the z-axis and microwave magnetic field H perpendicular z. The piezoelectric phase is poled with an electric field E_0 along z direction. We solve the equations of motion of magnetization for the ferrite. It is assumed that H_0 is high enough to saturate the ferrite to a single domain state for minimization of magnetic losses. The equation of motion of magnetization for the ferrite has the form:

$$\partial M/\partial t = - \gamma [M, H_{eff}], \qquad (9)$$

where $H_{eff} = - \partial ({}^{m}W)/\partial M$ and γ is the gyromagnetic ratio. For finding the effective magnetic

fields in the equation of motion of magnetization, we use the expression for the free-energy density ${}^{m}W$ for the ferrite that includes the Zeeman energy, crystalline anisotropy energy, magnetoelastic energy, and elastic energy. The stress components that appear in the expressions for magnetoelastic and elastic energy can be expressed in terms of dc electric field applied to the piezoelectric phase (as in Eq.1). Linearizing Eq. (9) enables one to get an expression for FMR frequency:

$$\omega = \gamma \left\{ \begin{array}{l} \left[H_3 + \sum_i \left(N_{11}^i - N_{33}^i \right) M_0 \right] \left[H_3 + \sum_i \left(N_{22}^i - N_{33}^i \right) M_0 \right] - \\ - \left(\sum_i N_{12}^i M_0 \right)^2 \end{array} \right\}^{1/2}, \qquad (10)$$

where $N^{i}{}_{kn}$ are demagnetization factors describing the shape anisotropy, crystalline anisotropy, and induced anisotropy due to ME interactions and (*1, 2, 3*) is a coordinate system in which the axis *3* is directed along the equilibrium magnetization as shown in Fig.1. Note that the dc electric field exerts an influence on FMR frequency via stress components in ferrite and the electric field contribution can be considered as induced magnetic anisotropy [32]. For the special case of bias field applied along the fiber length, the *E*-induced shift of FMR line is obtained as

$$\delta H_E = \frac{3\lambda \ {}^{m}T_3}{M_0}, \qquad (11)$$

with λ denoting the longitudinal magnetostriction constant and M_0 is the saturation magnetization for the ferrite. The term ${}^{m}T_3$ is a function of *E* and is determined by Eq. (1). The shift in the resonance field δH_E is given by

$$\delta H_E = \frac{3\lambda \ {}^{p}d_{33} v E}{M_0 [{}^{p}s_{33}(1-v) + {}^{m}s_{33} v]} \quad \text{and the ME coefficient} \quad \alpha_E = \delta H_E / E, \qquad (12)$$

where *v* is the volume fraction of PZT. Equation (12) enables one to obtain the *E* dependence

of FMR line shift and the ME coefficient.

Figure 6 shows estimates of α_E for fibers of ferrite core and PZT shell. Variation of the converse ME coefficient with the ratio of core-to-shell radius is shown for fibers with W- and Y- type ferrites. It is clear from Eq.(12) that a strong ME coupling at FMR is expected when (i) the piezoelectric volume fraction is sufficiently high, (ii) the piezoelectric component has a high d_{33} value and (iii) the magnetic phase has a high magnetostriction. Figure 6 shows that the highest α_E is estimated for Co_2W core-PZT shell structure. This is in contrast to low-frequency DME coupling strength which is maximum for Ni_2Y. This is accounted for by difference in the nature of direct ME effect at low-frequency and converse ME effect. The low-frequency and microwave ME effects are determined by piezomagnetic coefficient and magnetostriction constant, respectively. Fibers with rest of the hexaferrites are expected to have a weak ME effect compared to Co_2W-PZT core-shell nanostructure.

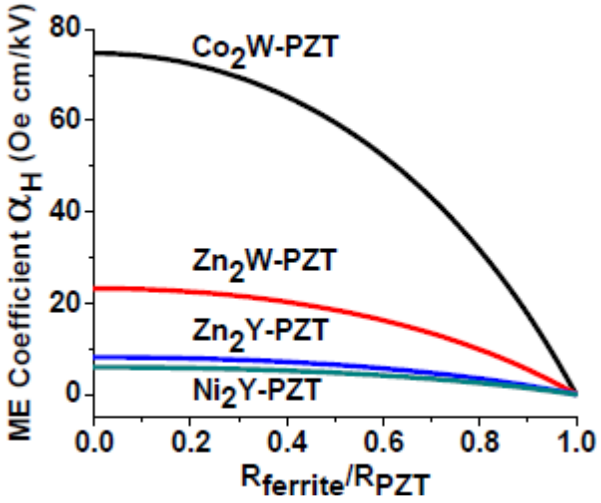

Fig.6. Converse ME coefficient α_E vs ratio of core-to-shell radius for hexaferrite -PZT nanofibers.

2.3 Assembly of Core-Shell Nanofibers

Superstructures of multiferroic nanofibers can be obtained by several techniques including magnetic and/or electric field assisted assembly and chemical self-assembly [23,33]. Such *2D*- and *3D*- structures are of particular interest for use in device technologies [34]. Here we consider the direct-ME coupling in a parallel array of core-shell fibers. For a free-standing fiber, magnetic core can be considered as homogeneously magnetized cylinder (with magnetization M along its axis) in self-bias or applied dc bias field. It is assumed that the magnitude of bias field corresponds to maximum in piezomagnetic coefficient. For an assembly of hexaferrite core-piezoelectric shell nanofibers, one should take into account the dipole-dipole interaction between magnetic cores. For simplicity, we restrict ourselves to the nearest neighbor approximation. The geometry of fibers is assumed to be uniform and the fibers are parallel to each other. The angle-dependent free energy includes Zeeman energy and dipole-dipole interaction energy. Assuming the radius of the fiber to be small compared to its length, one could use the following expression for interaction energy between two neighboring magnetic cores [35]

$$F_{12} = \frac{\mu_0}{2\pi}\frac{VM_{1z}VM_{2z}}{L^2 D}\left[1-\left(1+\frac{L^2}{D^2}\right)^{-0.5}\right] \tag{13}$$

with V and D being the core volume and separation between cores of nearest neighbor fibers and M_{1z} and M_{2z} are the magnetization along the z-direction for the magnetic cores of the two fibers. Assuming the periodic boundary conditions for the array, we can conclude that the equilibrium angles φ_m between the applied bias field and magnetization for neighboring magnetic cores are equal in value and opposite in sign. Minimization of free energy density in φ_m results in equilibrium magnetization direction.

The piezomagnetic coefficient q_{33} of ferrite core is proportional to Z-component of magnetization and thus proportional to $cos\ \varphi_m$. The induced voltage due to ME coupling

decreases in an array because of magnetic dipole interaction. Similarly, equilibrium orientation of PZT polarization is at an angle φ_e to the Z-axis. As a result, piezoelectric coefficient d_{33} decreases due to electric dipole interaction. Thus the ME voltage coefficient for an array is weaker by a factor $t = \cos \varphi_m \cos \varphi_e$ compared to a free standing fiber.

As an example, Fig.7 shows the low-frequency ME voltage coefficient $\alpha_{E,33}$ for Ni_2Y core-PZT shell nanofiber with a core radius of 100 nm and shell thickness varying from 10 nm to 100 nm. For the array of fibers the model predicts a reduction in the rate of increase in ME voltage coefficient with the shell thickness compared to free standing fiber. This is related to the fact that decreasing the shell thickness gives rise to a decrease in ferrite core separation and thus to an increase in magnetic dipole coupling strength. ME coefficient will approach the value for a free standing fiber for larger value of PZT shell thickness.

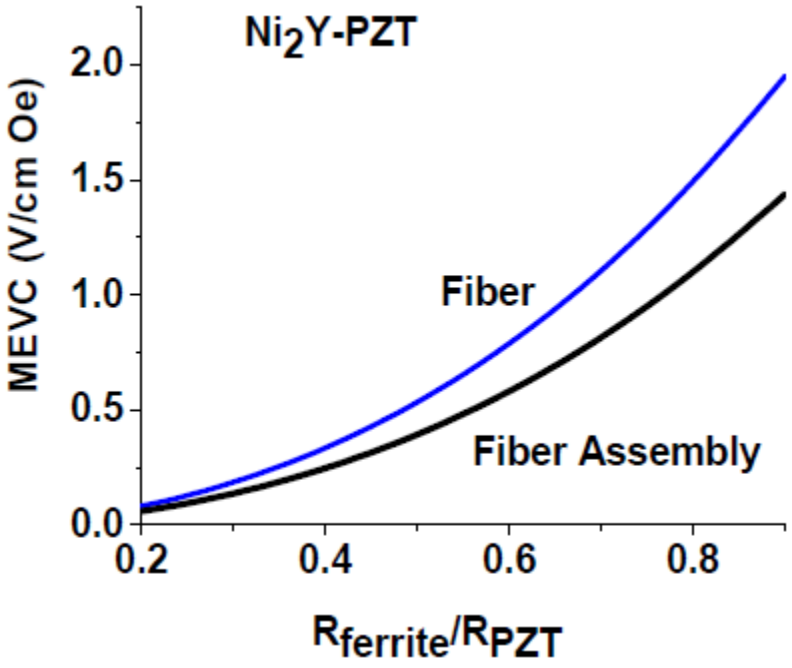

Fig. 7. Low-frequency ME voltage coefficient versus the ratio of ferrite-to-PZT radius for an assembly of nanofibers with 100 nm radius Ni_2Y core and PZT shell. ME voltage coefficient for a free standing Ni_2Y-NFO nanofiber is shown for comparison.

3. Discussion

We discuss next the modeling results presented in Sec.2 for direct- and converse-ME interactions in coaxial fibers of hexagonal ferrite and PZT. For direct-ME effect the key parameter of importance for the W- and Y-type hexaferrites is the piezomagnetic coefficient q. For converse-ME effect, hexaferrites with high magnetostriction and low FMR line-width are preferred since the measurements involve shift in FMR. Figures 2 and 3 show the low-frequency MEVC as a function of ratio of core radius-to-shell radius. The MEVC is the highest, 2.5 V/cm Oe, for fibers with Ni_2Y due to high q and the lowest, 100 mV/cm Oe, for fibers with Zn_2Y. The maximum value for MEVC is the same for fibers with PZT core or ferrite core. Another key inference from Figs. 2 and 3 is the prediction of maximum MEVC for PZT volume fraction of $v_p \sim 0.06$ for both kind of fibers, either with PZT-core or with PZT-shell. This relatively small volume fraction for PZT has to be compared with $v_p = 0.5$ for layered composites and can be attributed to the nature of mechanical connectivity, *(3,1)* for fibers and *(2,2)* for layered composites [30-32, 26]. The MEVC-values in Figs. 2 and 3 are much higher than theoretical estimates for bulk spinel ferrite-PZT composites with nm-sized inclusions of ferrite or PZT [36] and nickel ferrite-PZT nano bilayer, nanopillars or coaxial wires [27].

Enhancement in the ME coupling strength is anticipated for an ac magnetic field at the frequency of resonance modes. Results in Figs. 4 and 5 are for the direct-ME effect at EMR in the systems. For fibers of length 1 μm the MEVC at ~ 2.65 GHz is one to two orders of magnitude higher than the ME response of the systems at low frequency. Fibers with Ni_2Y have the strongest ME coupling and Zn_2Y systems have the weakest coupling, as is the case for low-frequency coupling. Results in Figs. 4 and 5 also have the following features that depart from those for the low-frequency ME coupling in the systems. For fibers with PZT-core, the maximum in MEVC occurs for $r_p = 0.4$, corresponding to a PZT volume fraction $v_p = 0.16$ whereas fibers with PZT-shell MEVC is the highest for $v_p = 0.1$. These v_p -values are much

higher than $v_p \sim 6\%$ for low-frequency ME coupling and is due to the dependence of v_p on the wavenumber k for acoustic modes associated with EMR (Eq.5). The peak MEVC for the hexaferrite-PZT fibers are comparable to predicted values for core-shell wires or nanopillars of NFO and PZT [26].

We modeled the strength of the converse ME effect in terms of the shift δH_E in the FMR absorption versus H profile due to a DC electric field E. Results in Fig.6 show $\alpha_H = \delta H_E/E$ as a function of $R_{ferrite}/R_{PZT}$ for fibers of hexaferrite core and PZT shell. One notices the highest α_E for fibers with very high shell radius (or volume fraction of v_p PZT) and is followed by a decrease α_E with decrease in v_p. Since α_H is directly proportional to the magnetostriction λ, α_E values in Fig.6 is maximum for fibers with Co_2W and is minimum for Ni_2Y. The key parameter for experiments on determination of α_H, however, is the line-width ΔH for FMR. Any E-induced shift δH_E in FMR has to be comparable or higher than ΔH. Amongst the hexaferrites considered in this work, single crystal Zn_2Y has the lowest $\Delta H \sim 50$ Oe [37] and is 210 Oe for Ni_2Y [38]. A recent study on FMR in polycrystalline Co-Zn-W reported ΔH = 1-4 kOe, depending on the concentration of Co and Zn [39]. Values of α_H in Fig.6 are orders of magnitude higher than measured values for layered composites of barium ferrite-PZT and nickel ferrite or yttrium iron garnet and PZT [9, 40].

Although the nanofibers considered are expected to show significantly stronger direct- and converse ME effects than bulk or thick film layered composites, device applications for the fibers may require assembly of the fibers into *2D*- or *3D*-films or similar superstructures that could be accomplished by techniques such as magnetic field and/or electric field assisted assembly. It is therefore necessary to model the ME interactions in such superstructures. In this work we considered the specific case of low-frequency ME effects in such assembly. Results in Fig.7 indicate a reduction in MEVC compared to free-standing fiber and is due to

magnetic and electric dipole-dipole interactions.

The theory and results in Sec.2 are based on the assumption of bulk material parameters for the fibers. It is therefore necessary to modify the theory with available magnetic and ferroelectric parameters for nanocrystalline ferrites and PZT. Feasibility of synthesis of the core-shell fibers is a key issue that needs to be addressed here. Coaxial fibers of spinel ferrites and PZT or barium titanate were reported in recent years by several techniques including electrospinning [21-23]. Puller, et al., reported on the synthesis of aligned fibers of M-, W-, Y- and Z-type hexaferrites [41]. In view of past success with synthesis of hexagonal ferrite fibers and coaxial fibers of spinel ferrites and PZT, one has to anticipate similar success in the synthesis of the core-shell nanowires considered in this study.

4. Conclusion

A model has been developed for ME interactions in a free-standing hexaferrite-piezoelectric nanofiber in the low-frequency, EMR, and FMR regions. Fibers of PZT and Ni_2Y are expected to have the highest ME voltage coefficient at low-frequency and at EMR. The strength of converse ME effect is characterized in terms of the shift of FMR in an electric field and is predicted to be maximum for Co_2W core-PZT shell structure. For an assembly of parallel hexaferrite-piezoelectric core-shell nanofibers, the low-frequency ME voltage coefficient is anticipated to increase with increasing PZT shell thickness due to the fact that increasing the shell thickness gives rise to an increase in ferrite core separation and thus to a decrease in magnetic dipole-dipole interactions. ME coefficient will approach the value for a free standing fiber for further increase in PZT shell thickness. The hexaferrite-PZT fibers are also expected to show the predicted ME responses under a self-bias due to high uniaxial or planar anisotropy field and are of importance for applications in sensors of magnetic fields.

Acknowledgments

The research at Oakland University was supported by grants from the Army Research Office (W911-NF-1210545) and the National Science Foundation (1307714). J. Zhang acknowledges support by the National Natural Science Foundation of China (Grant No. 61503344) and V. M. Petrov acknowledges support by the Russian Science Foundation (project no. 16-12-10158).

References

1. N. A. Spaldin, MRS Bulletin **42**, 385 (2017).

2. M. Fiebig, T. Lottermoser, D. Meier, and M. Trassin. Nature Reviews Materials **1**, 16046 (2016).

3. W. Zhang, R. Ramesh, J. L. MacManus-Driscoll, and H. Wang. MRS Bulletin **40**, 736 (2015).

4. S. Dong, J. M. Liu, S.W. Cheong, and Z. Ren, Advances in Physics **64**, 519 (2015).

5. J. Ma, J. Hu, Z. Li, and C. W. Nan, Adv. Mater. **23**, 1062 (2011).

6. J. Zhai, Z. Xing, S. Dong, J. Li and D. Viehland, J. Am. Ceram. Soc., **91**, 351 (2008).

7. G. Sreenivasulu, H. Qu, and G. Srinivasan, Materials Science and Technology **30**, 1625 (2014).

8. M. M. Vopson, Critical Reviews in Solid State and Materials Sciences **40**, 223 (2015).

9. N. X. Sun and G. Srinivasan, Spin **2**, 1240004 (2012).

10. X. Yang, Z. Zhou, T. Nan, Y. Gao, G. M. Yang, M. Liu, and N. X. Sun. Journal of Materials Chemistry C **4**, 234 (2016).

11. X. Zhuang, May-Tia Yang, Marc Lam Chok Sing, C. Dolabdjian, P. Finkel, Jiefang Li, and D. Viehland, IEEE Sensors Journal **16**, 662 (2016).

12. S. Fusil, V. Garcia, A. Barthélémy, and M. Bibes, Annual Review of Materials Research **44**, 91 (2014).

13. C. M. Leung, Xin Zhuang, Junran Xu, G. Srinivasan, Jiefang Li, and D. Viehland, Applied Physics Letters **109**, 202907 (2016).

14. M. T. Buscaglia, V. Buscaglia, L. Curecheriu, P. Postolache, L. Mitoseriu, A. C. Ianculescu, B. S. Vasile, Z. Zhe, and P. Nanni, Chem. Mater. **22**, 4740 (2010).

15. R. Liu, Y. Zhao, R. Huang, Y. Zhao, and H. Zhou, Journal of Materials Chemistry **20**, 10665 (2010).

16. G. Evans, G. V. Duong, M. J. Ingleson, Z. L. Xu, J. T. A. Jones, Y. Z. Khimyak, J. B. Claridge, and M. J. Rosseinsky, Adv.Funct. Mater., **20**, 231 (2010).

17. G. Sreenivasulu, V. M. Petrov, F. A. Chavez, and G. Srinivasan, Appl. Phys. Lett. **105**, 072905 (2014).

18. G. Sreenivasulu, T. A. Lochbiler, M. Panda, G. Srinivasan, and F. A. Chavez, AIP Advances **6**, 045202 (2016).

19. G. Dong, Z. Zhou, M. Guan, X. Xue, M. Chen, J. Ma, Z. Hu, W. Ren, Z. Ye, Ce-Wen Nan, and Ming Liu, ACS Nano **12,** 3751 (2018).

20. X. Tang, R. Viswan, M. Gao, C. M. Leung, C. Folger, H. Luo, B. Howe, J. Li, and D. Viehland, Scientific Reports **8**, 1628 (2018).

21. Z. H. Hua, P. Yang, H. B. Huang, J. G. Wan, Z. Z. Yu, S. G. Yang, M. Lu, B. X. Gu, and Y. W. Du, Mater.Chem. Phys., **107,** 541 (2008).

22. M. Liu, X. Li, H. Imrane, Y. J. Chen, T. Goodrich, Z. H. Cai, K. S. Ziemer, J. Y. Huang, and N. X. Sun, Appl.Phys.Lett., **90**, 152501 (2007).

23. G. Sreenivasulu, Maksym Popov, Ru Zhang, K. Sharma, C. Janes, A. Mukundan, and G. Srinivasan, Appl. Phys. Lett. **104**, 052910 (2014).

24. M. Popov, G. Sreenivasulu, V. M. Petrov, F. A. Chavez, and G. Srinivasan, AIP Advances **4**, 097117 (2014).

25. G. Sreenivasulu, V. M. Petrov, F. A. Chavez, and G. Srinivasan, Applied Physics Letters **105**, 072905 (2014).

26. V. M. Petrov, G. Srinivasan, M. I. Bichurin, and A. Gupta, Phys. Rev.B **75**, 224407 (2007).

27. V. M. Petrov, M. I. Bichurin, and G. Srinivasan, J. Appl. Phys. **107**, 073908 (2010).

28. Landolt-Bornstein; Numerical data and functional relationships in science and technology, Group III, Crystal and Solid State Physics, vol 4(b), Magnetic and Other Properties of Oxides, eds. K.-H. Hellwege and A. M. Springer, Springer-Verlag, New York (1970).

29. R. Pullar, Progress in Materials Science 57, 1191 (2012).

30. G.Harshe, J.O.Dougherty, R.E.Newnham, Int. J. Appl. Electromagn. Mater., **4**, 145 (1993).

31. M.I.Bichurin, V.M.Petrov, and G.Srinivasan, Ferroelectrics, **280**, 165 (2002).

32. M.I.Bichurin, V.M.Petrov, and G.Srinivasan, Phys. Rev., B **68**, 054402 (2003).

33. M Grzelczak, Jan Vermant, Eric M. Furst, and Luis M. Liz-Marzán, ACS Nano **4**, 3591 (2010).

34. X. Shi, Weiping Zhou, Delong Ma, Qian Ma, Denzel Bridges, Ying Ma, and Anming Hu, Journal of Nanomaterials **16**, 122 (2015).

35. .R. Piccin, D. Laroze, M. Knobel, P. Vargas and M. V´azquez, Euro. Phys. Lett., **78, 67004** (2007).

36. V. MPetrov, M. I. Bichurin, V. M. Laletin, N. Paddubnaya, and G. Srinivasan, Magnetoelectric interaction phenomena in crystals-NATO science series II, **164**, 65 (2004).

37. L. M. Silber, C. E. Patton, and H. F. Naqvi, J. Appl. Phys. **54**, 4071 (1983).

38. R. A. Barden, I. Gordon, R. L. Harvey, IEEE Trans. Magn. **MAG-2**, 43 (1966).

39. E. P. Naiden, E. P., V. A. Zhuravlev, V. I. Suslyaev, R. V. Minin, V. I. Itin, and E. Yu Korovin, International Journal of Self-Propagating High-Temperature Synthesis **20**, 200 (2011).

40. G. Srinivasan, I. V. Zavislyak, and A. S. Tatarenko. Applied physics letters **89**, 152508 (2006).

41. R. C. Pullar, R. C., S. G. Appleton, M. H. Stacey, M. D. Taylor, and A. K. Bhattacharya. Journal of Magnetism and Magnetic materials 186, 313 (1998).